Acta Astronautica 197 (2022) 107–114

Contents lists available at ScienceDirect

Acta Astronautica

journal homepage: www.elsevier.com/locate/actaastro

Research paper

Simultaneously measured direct and indirect thrust of a FEEP thruster using novel thrust balance and beam diagnostics

Nina Sarah Mühlich [a,b,*], Joachim Gerger [b], Bernhard Seifert [b], Friedrich Aumayr [a]

[a] TU Wien, Institute of Applied Physics, Vienna, 1040, Austria
[b] FOTEC Forschungs- und Technologietransfer GmbH, Wr. Neustadt, 2700, Austria

ARTICLE INFO

Keywords:
Beam diagnostics
Direct thrust
Electric propulsion
Faraday cup
FEEP thruster
Indirect thrust
Steady state null balance
Torsion thrust balance
Voice coil actuator

ABSTRACT

For the characterisation of an electric propulsion system, the determination of the thrust has a crucial role. The thrust of an Indium FEEP Multiemitter (IFM) Nano Thruster laboratory model is measured directly with a thrust balance and indirectly via beam diagnostics. Both measurements are carried out simultaneously to enable mutual verification with high accuracy. The novel mN-torsion thrust balance by FOTEC resolves six different thrust magnitudes, ranging from 10 μN to 1 N. It is based on the so-called force-feedback method using a voice coil actuator to determine the thrust, which leads to an accuracy of better than 2 %. The indirect thrust measurements were performed with a high-precision beam diagnostics system by FOTEC. A semi-circular diagnostics arm equipped with 23 digital Faraday cups is used to measure the ion current density distribution of the entire beam. The thrust results of both systems show an agreement with a deviation less than 5 % for thruster operation points ranging from 50 to 450 μN. This proves that the performance of a FEEP thruster can be characterised very precisely by indirect trust measurements.

1. Introduction

Field emission electric propulsion (FEEP) thrusters are playing an increasingly important role in the space sector, especially the Indium FEEP Multiemitter (IFM) Nano Thruster. The IFM Nano Thruster, shown in Fig. 1, was developed at the research company FOTEC and commercialised by the space tech company ENPULSION, both located in Austria. FEEPs have a wide range of application areas, like as CubeSat propulsion or for science and Earth observation missions [1,2]. Thereby, they are used for drag free and fine altitude control or as a clustered version as main propulsion system of a spacecraft, which includes station keeping, orbital raising and drag compensation. In order to be able to comply with the requirements of the different application areas, a performance characterisation of the thruster is necessary.

Direct and indirect thrust measurements are commonly used methods to analyse the performance of an electric propulsion (EP) thruster. The thrust of different EP technologies can be determined directly using a thrust balance. For this purpose, typically pendulum balances are used [3–10], such as a horizontal μN torsion balance developed by FOTEC in 2013 [11,12]. This balance is especially suitable for high voltage (< 20 kV) and high current (< 3 A) electric propulsion systems. Since 2013, it has received several upgrades, to be able to cover a thrust range over several orders of magnitude with high accuracy. This was achieved by converting the deflection measurement into a force-feedback mode, which is also known as steady state null balance [13].

Alternatively, the thrust of an ion thruster can be determined indirectly from its beam properties. For this purpose, certain key parameters are required, like beam shape, ion energy distribution and fraction of multiply charged particles. When calculating the thrust, it is of elementary importance how precisely these parameters can be determined. For ion thrusters, these parameters are usually distribution functions, depending on the operation point. In addition, they are influenced by chamber effects, which distorts the calculated thrust. Due to these two effects direct thrust measurements are usually preferred in order to qualify an EP thruster.

However, in this paper it will be shown that for FEEP thrusters the parameters can be determined precisely leading to an accurate indirect thrust calculation. In order to prevent influences on the beam, like charge exchange effects or beam widening, a sufficiently large high vacuum facility is used. Another advantage of indirect measurement is the access to other key parameters that play an important role in the characterisation of an EP thruster. This includes the beam divergence angle, which is required to analyse the spacecraft-beam interaction. Furthermore, the thrust vector alignment can be computed, which is particularly important for a precise spacecraft altitude control.

* Corresponding author at: TU Wien, Institute of Applied Physics, Vienna, 1040, Austria.
E-mail addresses: muehlich@fotec.at (N.S. Mühlich), gerger@fotec.at (J. Gerger), seifert@fotec.at (B. Seifert), aumayr@iap.tuwien.ac.at (F. Aumayr).

https://doi.org/10.1016/j.actaastro.2022.05.009
Received 17 January 2022; Received in revised form 28 April 2022; Accepted 7 May 2022
Available online 21 May 2022

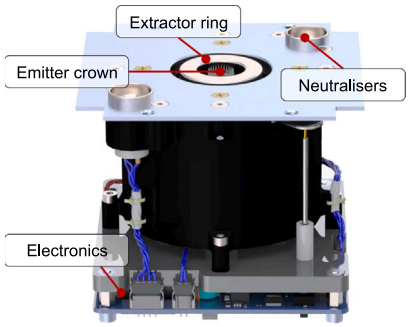

Fig. 1. Drawing of an IFM Nano Thruster with indicated main components.

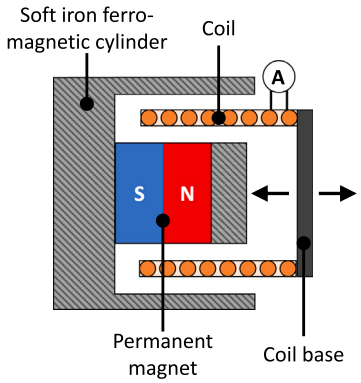

Fig. 2. Schematic drawing of the used voice coil actuator (VCA), consisting of a permanent magnet and a coil driven by a current-controlled power supply (A).

Direct thrust measurements in combination with full beam diagnostics measurements are rarely done. In this process, many inaccuracies could arise when comparing the results of the two separate systems. In this paper, both, indirect and direct thrust measurements methods are performed simultaneously at an IFM Nano Thruster laboratory model. For the direct thrust measurements, the newly developed mN-torsion pendulum thrust balance is used, which is presented the first time in this configuration. The indirect thrust measurements are carried out with an upgraded digital beam diagnostics system [14]. It is shown that the results of the direct and indirect thrust measurements have a high level of agreement. This allows to verify the data obtained from both systems at the same time and helps to reduce measurement uncertainties.

With this knowledge, the electrostatic beam simulation model developed in 2020 can predict the thrust of any new FEEP thruster geometry [15].

2. Analytical methods

2.1. Direct thrust measurements

For direct thrust measurements of an EP thruster pendulum thrust balances are typically used. Thereby, the produced thrust can be computed from the deflection of the balance arm. However, there is also a second possibility in which the balance arm is held stationary in the centre, which is known as steady state null balance or force compensation method. For the presented thrust balance, this is done through a so-called voice coil actuator (VCA), which uses Lorentz forces to generate actuation. A schematic drawing of the used VCA is shown in Fig. 2. It consists of an axially magnetised cylindrical permanent magnet and a moving coil, which is located in a ferromagnetic cylinder. The applied current generates a magnetic field which exerts a force on the permanent magnet. The generated force T is proportional to the applied current I:

$$T = I \int dl \times B = f \cdot k \cdot I + b\,[\mathrm{N}], \tag{1}$$

where l represents the geometry of the solenoid and B the magnetic flux in the permanent magnetic field. A conversion factor of f=3.89 N/A is specified by the VCA supplier to convert the applied current into a force. The gain-factor k and the offset b are determined by the calibration procedure of the VCA. For calibration, the VCA permanent magnet is placed on a weight scale. The coil is positioned with a stamp at a minimum distance exactly above the magnet. A current is applied to the coil, which is increased successively. At the same time the mass change on the weight scale is measured and can be converted into force. In this way, a calibration fit-curve can be created to determine the parameters k and b, as will be shown in Section 4.1.

2.2. Indirect thrust measurement

The thrust produced by an ion thruster can also be calculated from its beam properties, known as indirect thrust measurement:

$$T = I_{em} \cdot \sqrt{\frac{2\ m \cdot \eta_v \cdot V_{em}}{e}} \cdot \alpha \cdot \gamma, \tag{2}$$

where I_{em} is the emitter current, m/e the mass to charge ratio and V_{em} the emitter voltage. The thrust correction factors are η_v acceleration efficiency, γ divergence efficiency and α multiply charged species term [16].

The α factor considers the fraction of multiple charged ions, which are commonly observed in electric thrusters [16]. Fehringer did magnetic mass spectrometry investigations of a needle type FEEP thruster, which was the predecessor of the IFM Nano Thruster [17]. He analysed that single charged indium ions make up 98 % of the total emitted current. Other electric thruster types produce a larger number of multiple charged ions, such as a High Efficiency Multistage Plasma Thruster (HEMPT) ion beam consists with 60 % of doubly and triply charged ions [18].

The correction factor η_v includes the ion acceleration efficiency. This efficiency was observed with a retarding potential analyser (RPA) [15,19]. Thereby, it was analysed that the energy of the ions corresponds exactly to the emitter voltage V_{em}, independent of the spatial angle. In the case of Hall Effect Thrusters (HET), there is a spread in beam energies produced in the thruster [16,20]. Or for example for HEMP thrusters the ion energy varies dependent on the plume angle [21].

The divergence efficiency coefficient γ includes the cosine loss effects on the beam current I_{em} due to the divergence of the beam. For this the spatial ion current density distribution over the entire beam has to be integrated:

$$\gamma = \frac{1}{I_{em}} \cdot \sum_{ij} I_{ij} \cdot \cos\theta_i \cdot \cos\phi_j, \tag{3}$$

where θ and ϕ are the spherical coordinates of a hemisphere in front of the beam. The current density I is typically measured with Faraday cups. A large vacuum facility is particularly suitable for measuring the beam with highest precision. For example, the beam can be influenced by the potentials of the facility walls. Furthermore, a high pumping rate is beneficial, as this reduces the charge exchange effects of wall reflected species that could distort the current measurement of the Faraday cups.

In summary, the IFM Nano Thruster has a mono-energetic, singly-ionised beam ($\alpha = 1$ and $\eta_v = 1$). Therefore, only the divergence efficiency γ has to be considered for the indirect thrust computation. This efficiency is analysed with the high precision beam diagnostics system.

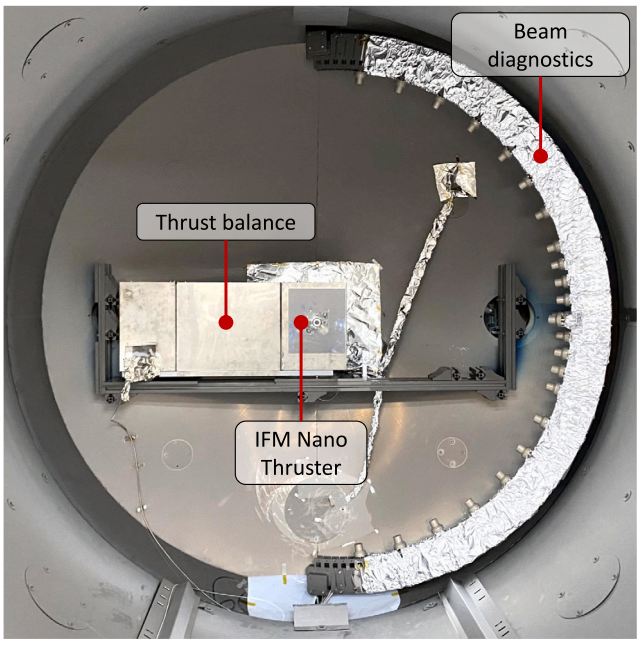

Fig. 3. Combined test setup with IFM Nano Thruster test module mounted on mN-thrust balance and semi-circular beam diagnostics arm equipped with 23 Faraday cups.

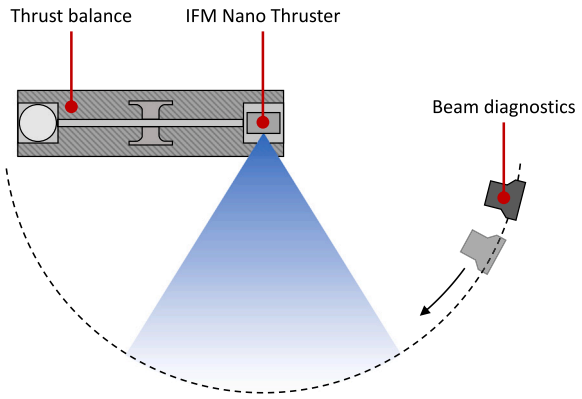

Fig. 4. Top view sketch of combined setup with IFM Nano Thruster attached on thrust balance combined with beam diagnostics.

3. Direct and indirect thrust measurement setup

Two different thrust measurement setups were used at the same time, located in FOTEC's large vacuum facility as shown in Fig. 3. Therefore, no setup change between the measurements is carried out, which avoids air cycles or system conversions that could lead to inaccuracies. The vacuum facility has a length of 3 m, a diameter of 2.2 m and reaches during nominal thruster operation a pressure of $2 \cdot 10^{-7}$ mbar. In this test setup, both the direct and the indirect thrust of an IFM Nano Thruster test module are to be determined simultaneously. The thruster is located on the mN-thrust balance, which is protected by a shield against back sputtering. A semi-circular diagnostics arm equipped with 23 Faraday cups is used to measure the ion current density distribution of the thruster beam in 1 m distance. The thrust balance is mounted in such a way that the thruster emitter is exactly centred in the semi-circle of the diagnostics arm. A sketch of both combined setups is shown in Fig. 4. Both measurement setups are described separately in the following subsections.

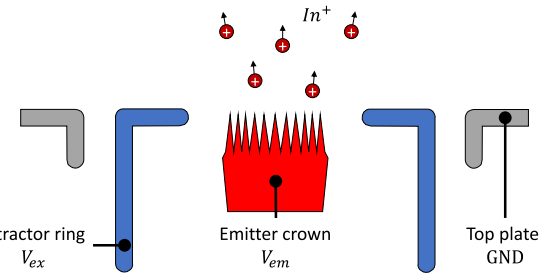

Fig. 5. IFM Nano Thruster simplified as schematic drawing with positive emitter and negative extractor electrode.

3.1. IFM Nano Thruster description

The IFM Nano Thruster is based on the field emission principle, where ions are emitted from a liquid metal by means of strong electric fields [12]. A schematic drawing of the IFM Nano Thruster is shown in Fig. 5. The core of the thruster is a porous tungsten crown with 1 cm diameter consisting of 28 needles, wetted with liquid indium. Each of these needles acts as a separate ion emission source, where the term 'multiemitter' is originated. This configuration results in a higher achievable total emission current. A positive high voltage is applied to the crown emitter and a negative high voltage at the ring-shaped extractor. Due to the strong electric fields at the needle tips, ions are produced and accelerated. The ions are accelerated along the electric field, which produces the thrust. For the experimental tests performed in this paper, a laboratory model of the IFM Nano Thruster was used.

3.2. Thrust balance setup

A schematic drawing of FOTEC's novel mN-thrust balance is shown in Fig. 6. It consists of an horizontal 80 cm long arm suspended by two spring bearings in the centre, which ensures frictionless deflection of the arm. The pivot frame is retaining the spring bearings ensuring low thermal drift, high reproducibility and ultra-low noise levels. On the right balance table, the IFM Nano Thruster test module is located and on the left side the counterweight with equal mass. This ensures cancellation of the overall torque and prevents bearings from absorbing shear forces. The total capacity of the thrust balance is 15 kg on each table.

An optical displacement sensor measures the distance between the sensor and the mirror mounted on the arm. The thrust balance is operated in force-feedback mode, where the arm is kept in its centre position. This is realised with the main voice coil actuator (VCA), which is located underneath the counterweight table. The VCA permanent magnet is mounted on the balance arm and the voice coil is mounted on a support in front of the arm. This avoids current supply connections to the balance arm. The VCA compensates the force generated by the thruster, which allows the computation of the generated thrust, as described in Section 2.1. A software-based control loop is used to control the force actuator. Depending on the thrust transients, thrust level and thruster mass, the PID controller values can be adjusted for improved results, such as faster response, low overshoot or low noise [22]. A second auxiliary VCA is used to test the balance with a known force. Thereby, the auxiliary VCA simulates a thrust by applying a test force. This allows a direct verification and calibration of the thrust balance. The VCAs are located behind the balance arm, to ensure that for both the force vector points in the same direction and can therefore be compared more accurately.

The thrust balance is equipped with a magnetic damping system. It consists of an eddy current brake to reduce measurement noise and long-lasting oscillations caused by an over- or undershoot. The damping rate can be varied by shifting the damping system along the arm, which

Table 1
MN-thrust balance key specifications.

Parameter	Size
Thrust range	0–1 N
Measurement ranges	<0.01, 0.1, 1, 10, 100, 1000 [mN]
Accuracy	2% of measurement range
Noise floor	15 μN RMS
Sensitivity	1.66 μN/μm
Dimensions	800 × 200 × 374 mm (L × W × H)
Max. load	15 kg

Table 2
Digital Faraday cup system key specifications.

Parameter	Size
Current density range	<3.8 μA/cm^2
Accuracy	±5 pA/cm^2
Sampling frequency	7–3520 Hz
Horizontal resolution	>0.1°
Vertical resolution	4°–12°
Repeller	−80–0 V

is particularly suitable for pulsed thrusters. For the characterisation of continuous electric propulsion systems such as FEEP, Hall or gridded ion thrusters the low response rate has no influence on the results. Alternatively, a software based damping system can be used, which was developed for the new thrust balance. During this test only the software based damping system is used.

Standard electrical feed-troughs (F/T) cannot be used to supply or read out the thruster. Thin cables could heat up at higher currents and generate a phantom force. This common effect is mitigated by using a conductive liquid to connect the lead wires on the movable part of the balance with the electrical connections outside the test facility.

The thrust balance is also equipped with a gas propellant system, so that it can also be used for other thruster types with gas supply. Special tube holder and ultra-flexible tubes ensures minimal influence of thrust measurement accuracy. Since the IFM Nano Thruster includes a solid indium propellant tank, no gas feeding system is used during this test.

The mN-thrust balance key specifications are shown in Table 1. The balance has a variable measurement range up to 1 N, where six different thrust ranges can be used, making it suitable for a variety of thruster types. The VCA controller support different current ranges and the most suitable is automatically selected by the firmware.

The measurement accuracy is the difference between the measured and the commanded thrust. Error propagation has shown that the VCAs have the major contribution to the accuracy, which results in 2 % of the respective measurement range.

The resolution is defined as the smallest measurable difference between two thrust inputs. In practice, the resolution is limited by the noise floor of the thrust measurement [13]. The noise floor is the same for all measurement ranges with 15 μN RMS (also shown in Section 4.1).

Typically, the sensitivity s is also given for a thrust balance, which is described as the deflection of the balance arm x for a given applied force F: $s = dx/dF = r^2/D$. Since the mN-thrust balance is operated in the force-feedback mode where the arm is stationary in the centre, the sensitivity is here defined by a combination of the spring constant D and the arm length r. A Philtec DMS D64 is used as an optical displacement sensor. It has an accuracy of ±1 μm in the far field, which corresponds to 1.6 μN and is included in the balance accuracy.

3.3. Beam diagnostics setup

In 2021 FOTEC developed an upgraded beam diagnostics system for high spatial resolution of an ion beam in polar and azimuthal direction [14]. The diagnostics system consists of 23 digital Faraday cups (DFC) and one retarding potential analyser (RPA). These are

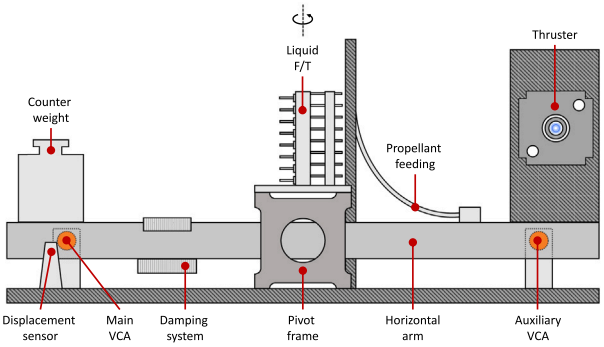

Fig. 6. Schematic drawing of FOTEC's novel mN-thrust balance.

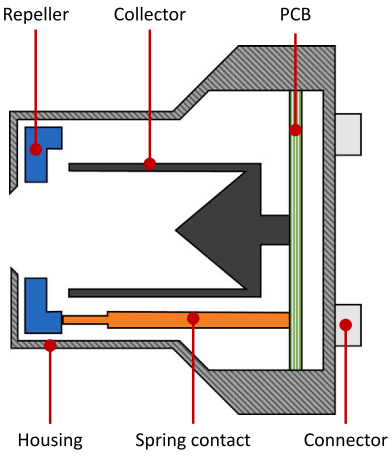

Fig. 7. Schematic drawing of a digital Faraday cup.

mounted on the semi-circular diagnostics arm as shown in Fig. 3. With the Faraday cup system, the ion or electron current density distribution of a particle beam can be measured. The entire measuring electronics is located in the head of the DFC. This allows high precision measurements of the beam current density, since signal interference due to cable length or movement of the diagnostics arm can be eliminated. Furthermore, the DFCs automatically switch between different current ranges. Thus, the optimal resolution is archived for thrusters of different power ranges and current densities. In Fig. 7 a schematic drawing of a digital Faraday cup can be seen. In the geometric design, the widening of the beam is considered, which means the entrance aperture has the smallest diameter. Sputtering effects in the area of the entrance aperture are reduced by a bevelling structure. A cup-shaped collector measures the current caused by impinging ions or electrons. In addition, the cup has a conical structure to trap secondary electrons. The negative biased repeller electrode prevents ambient electrons or slow charge exchange ions from entering the cup. These slow ions are attracted to the orifice and do not contribute to the measured current. Furthermore, secondary electrons triggered by ion bombardment are prevented from leaving the cup. Other Faraday cup studies for FEEP thrusters came to a similar geometric design [23] or also feature built-in electronics for signal processing [21]. A major advantage compared to other beam diagnostics systems is that the measurement and control electronics is integrated in the head of the DFC on a printed circuit board (PCB). For the application of FEEP thrusters, the structure of the DFC insulators considers the deposition of indium, which could lead to conductive connections.

The 23 DFCs are attached to the semi-circular diagnostics arm with different spacings to have a higher resolution in the beam centre. The key specifications of the DFC system are presented in Table 2. All DFCs

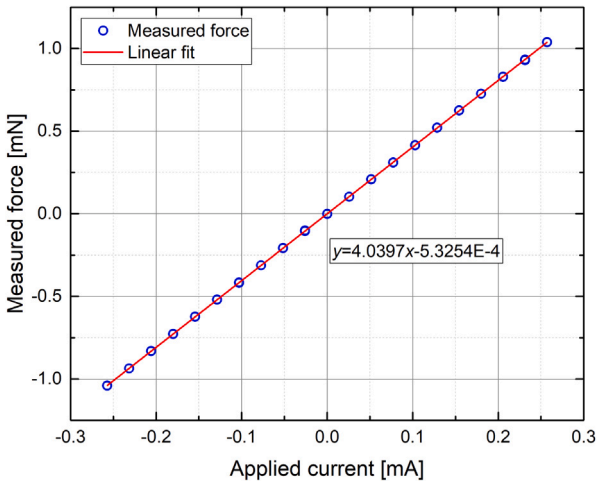

Fig. 8. Voice coil actuator (main) calibration curve for <1 mN thrust range with linear fit-function.

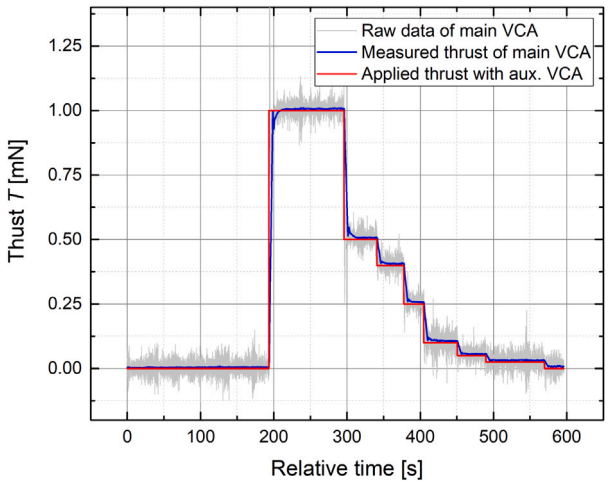

Fig. 9. Thrust balance verification at <1 mN thrust range, installed on mN-thrust balance.

are triggered to sample and convert the signal at the same time the rotation in 1° steps from −80° to 80° in 90 cm distance around the thruster. With this the measured ion current density is mapped on a spherical surface mesh [15]. Typical beam properties can be analysed from the 3D measurement data. This includes total beam current and the thrust vector. Furthermore, the divergence half-cone angle can be computed, defined as angle from the thrust vector which contains 95% of the total beam current.

4. Results

The IFM Nano Thruster test module was operated at different operation points by varying the emitter current I_{em}, emitter voltage V_{em} and extractor voltage V_{ex}. At every operation point direct thrust measurements were performed for 5 mins and an average value was formed. A beam diagnostics scan was carried out afterwards which took ~20 mins. Previous analyses have shown that the beam remains stable over time, which is also shown in Section 4.2. Therefore, measurements were made with a higher resolution [15]. The measurements of the two systems were performed successively for each point, so that the direct thrust measurement is not disturbed by the movement of the diagnostics arm. In the following, the respective results of the two systems are shown and compared thereafter.

4.1. Thrust balance results

Before starting with the thrust balance measurements the two voice coil actuators (VCA) were calibrated with the procedure described in Section 2.1. The recorded calibration curve for the thrust measurement range <1 mN is shown in Fig. 8. The measured weight force is plotted against the applied voice coil current. From the linear fit of the data points a gain factor of $k = 4.0397/3.89 = 1.0385$ and an offset of $b = 5.325 \cdot 10^{-7}$ N could be observed. These parameters are used as input parameters for the VCA firmware, which uses equation (1). With this the required VCA current to compensate the force of the thruster can be computed into direct thrust. Subsequently the parameters were verified in the same setup, by repeating the thrust measurement using the software with the identified calibration factors. A maximum peak-to-peak deviation of 10 μN and an RMS of 5 μN were achieved, which is within the expected accuracy of the thrust balance.

The two calibrated VCAs were installed on the mN-thrust balance in the test setup described in Section 3.2. Next step was the verification of the VCAs calibration data. For this purpose, a test force is applied using the auxiliary VCA. At the same time, the main VCA counteracts the applied force of the auxiliary VCA with a certain current. With the current and the previously identified calibration factors the required thrust is computed using equation (1). The two results are compared with each other, which can be seen in Fig. 9. The red curve shows the applied thrust of the auxiliary VCA and the blue curve the measured thrust with the main VCA. The following forces were applied in succession: 0, 1000, 500, 400, 250, 100, 50, 20, 0 μN. It can be identified that the main VCA reacts immediately to the applied force without overshooting. The comparison between commanded and measured thrust results in a deviation of <20 μN (≈2 %), which describes the accuracy of the thrust balance. The noise floor corresponds to the RMS of 15 μN and can be reduced by longer measurement time.

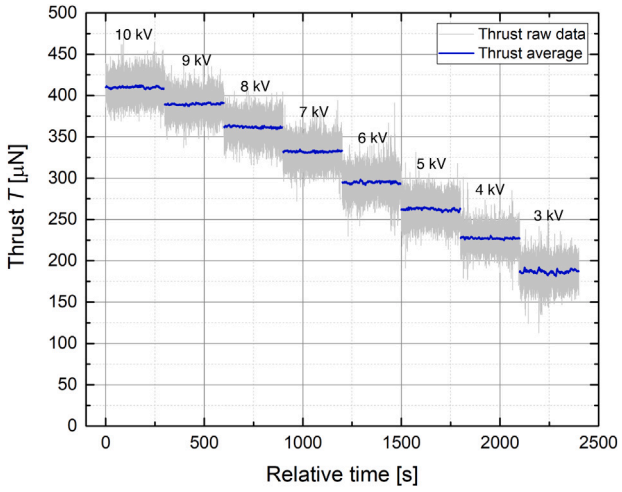

Fig. 10. Direct thrust measurement at constant emitter current I_{em} = 3.5 mA and stepwise variation of emitter voltage V_{em} from 10 down to 3 kV.

Direct thrust measurements of an IFM Nano Thruster test module were performed using the mN-thrust balance including the two calibrated and verified VCAs. The measurement data was recorded for every thruster operation point for 5 mins with 0.05 s sample interval. An average value was formed over 100 data points. Both results can be seen in Fig. 10. This series of measurements was taken at a constant thruster emitter current of 3.5 mA, which corresponds to the nominal operation of an IFM Nano Thruster. In order to vary the thrust, the emitter voltage was gradually reduced from 10 kV down to 3 kV. Further

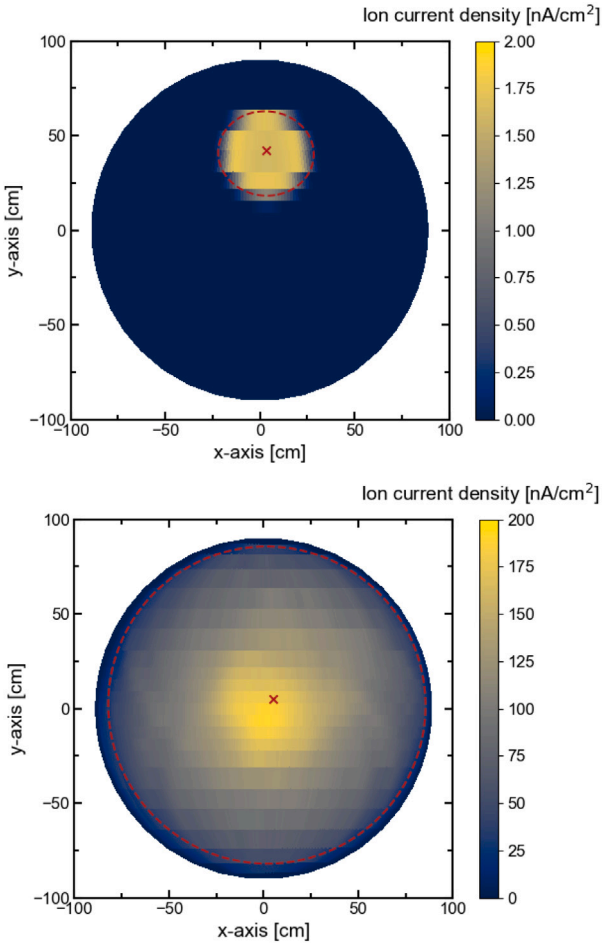

Fig. 11. Example of beam profiles at IFM Nano Thruster emission current of I_{em}=5 μA (top) and I_{em}=3.5 mA (bottom).

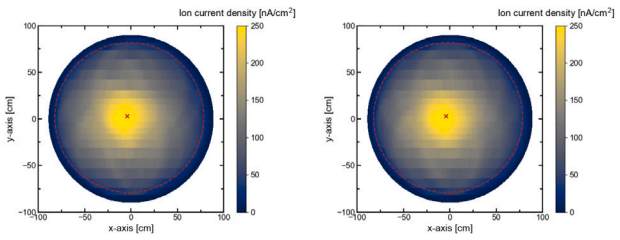

Fig. 12. Example of beam profile stability over time with measurement interval of 1.5 h at IFM Nano Thruster emission current of I_{em}=3 mA.

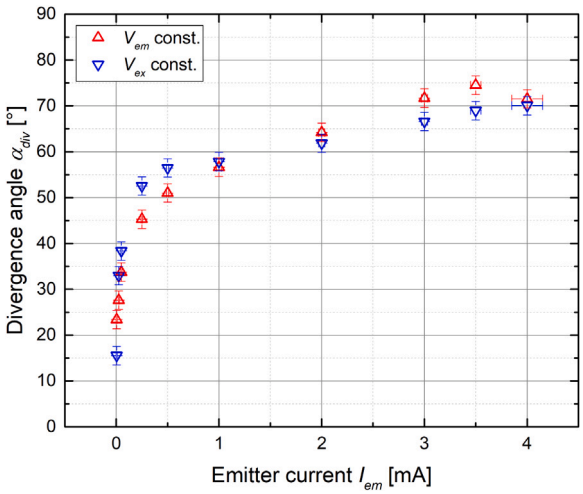

Fig. 13. Measured divergence angle for different thruster emission currents at constant emitter voltage (red) and constant extractor voltage (blue).

measurements were carried out at constant emitter voltage as well as at constant extractor voltage. The results are presented and compared with the beam diagnostics results in Section 4.3.

4.2. Beam diagnostics results

Beam diagnostics measurements of an IFM Nano Thruster test module were performed with the system described in Section 3.3. The diagnostics arm was moved in steps of 1° from −80° to 80° around the thruster and 10 data points were recorded at each position. The spherical data recorded with the semi-circular diagnostics arm can be projected into Cartesian coordinates to visualise the beam profile. The beam properties are calculated on the basis of the three-dimensional data and are displayed visually in the projected beam profile. Fig. 11 (top) shows a beam profile measured at an minimum thruster emission current of I_{em} = 5 μA. This value lies outside the usual operation of an IFM Nano Thruster. It is shown to demonstrate the high resolution of the DFC system, where a maximum ion current density of ~2 nA/cm² was measured. It shows the profile of a single emitting needle located in the upper part of the emitter crown. The beam diagnostics analysis software indicates the computed thrust vector with a cross. The divergence half-angle α_{div} is represented with a dashed circle.

Fig. 11 (bottom) shows a beam profile measured at a nominal thruster emission current of I_{em} = 3.5 mA. A maximum ion current density current of ~200 nA/cm² was measured. Here the individual beamlets coming from the 28 emitting needles can be diagnosed. With this the beam divergence angle of the whole beam profile (α_{div} = 69°) consisting of 28 single beamlets is larger than of a single emitting needle (α_{div} = 17°) in Fig. 11 (top).

Fig. 12 shows the time-dependent beam stability of an IFM Nano Thruster laboratory model with a measuring interval of 1.5 h. Thereby, the beam divergence angle varies by less than 0.07°.

According to Section 2.2, the divergence coefficient γ is necessary to compute the indirect thrust. The divergence angle is related to the γ-coefficient, which is why it is examined in more detail. In Fig. 13 the computed divergence angles α_{div} for different emitter current I_{em} values are shown. The red data points show the divergence angle at constant emitter voltage and the blue data points at constant extractor voltage. The emitter needles require a certain field strength to ignite. For this reason, with increasing emitter current the number of emitting needles increases which in turn increases the divergence angle. Furthermore, the space charge in front of the emitter increases with higher emission current, which leads to a beam widening. When comparing the two data series, a larger increase is noticeable for V_{em} constant in the range between 0.5 to 4 mA. In this series, a higher emitter current is achieved by increasing the negative extractor voltage. By increasing the negative voltage, the positive ions are drawn outwards and the beam expands, which explains the increased divergence angle.

The total beam current I_{tot} was calculated by integrating the current density of the entire beam profile and compared with the beam emission current I_{em}. The deviation between I_{tot} and I_{em} is always below 0.2 mA. In terms of percentage, the deviation decreases with increasing current, which is shown in Fig. 14. In the nominal ion emission operating range of the IFM Nano Thruster (2–4 mA), the deviation is always <5 %. For lower emission currents the integration becomes less accurate over the entire beam profile. Thereby it has to be considered, that the set emitter current has an error between 6–150 μA. Consequently, a deviation of 24% results for 25 μA emission current.

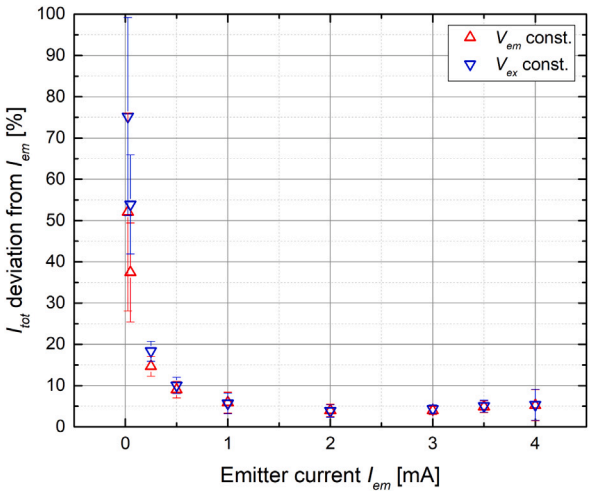

Fig. 14. Deviation of integrated total current I_{tot} from the thruster emitter current I_{em}.

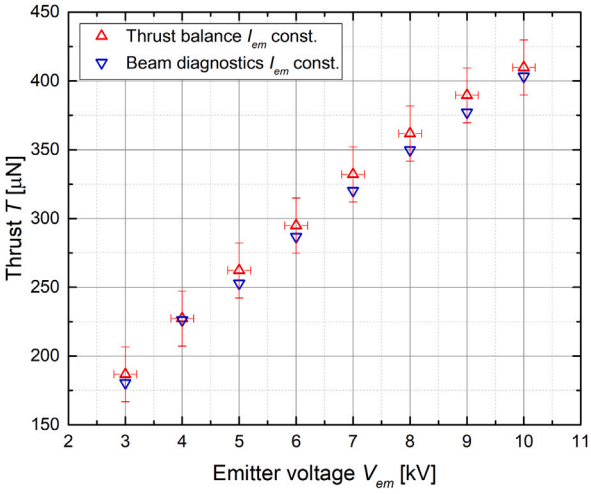

Fig. 15. Comparison of direct (red) and indirect (blue) thrust measurements at constant thruster emitter current $I_{em} = 3.5$ mA and different emitter voltages.

For the indirect thrust calculation, the γ-coefficient is calculated with equation (3) from the beam diagnostics data. With this the thrust can be computed according to equation (2).

4.3. Comparison of direct and indirect thrust measurement results

The direct and indirect thrust measurement results of sections 4.1 and 4.2 are compared in the following. Fig. 15 shows thrust measurement comparison during a thruster emitter voltage sweep at constant emitter current of 3.5 mA. Both data series show a thrust increase with increased emitter voltage. According to equation (2) the thrust is proportional to the square root of the emitter voltage V_{em}. On average of all data points the measured direct thrust is ~8.5 µN larger than the indirect thrust, which corresponds to ~2.8 %. This inaccuracy can be explained mainly with the vertical inaccuracy of the beam diagnostics system, as the digital Faraday cups are positioned at a certain distance, as described in Section 3.3. In future, the diagnostics system will be upgraded by using a DFC array to increase the vertical resolution. However, the beam diagnostics results are all within the accuracy range of the thrust balance (<20 µN). In addition to the emitter voltage sweep, an emitter current sweep was carried out as can be seen in Fig. 16. Thereby, once the emitter voltage was kept constant and afterwards the extractor voltage. All four data series show an increase

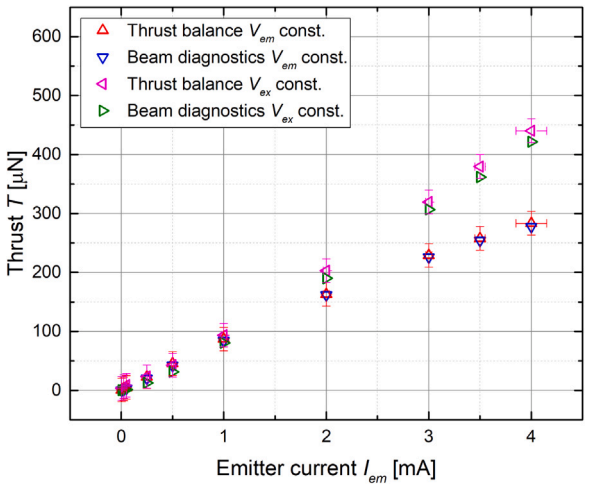

Fig. 16. Comparison of direct and indirect thrust measurements at constant thruster emitter voltage $V_{em} = 5$ kV (red and blue) and constant extractor voltage $V_{ex} = -5$ kV (magenta ad green) at different emitter currents I_{em}.

in thrust with an increase in current. According to equation (2) the thrust is proportional to the emitter current. However, the V_{ex} constant data series has a stronger thrust increase than the V_{em} constant series. This behaviour has two causes. For the data series V_{ex} constant, the emitter voltage V_{em} had to be increased to achieve a higher current. However, this value is also included in the thrust equation (2) and therefore leads to an additional thrust increase. In the data series with V_{em} constant, V_{em} has no influence on the thrust change. However, there is no linear increase in thrust with current, because the curve flattens with increased emitter current. This can be explained with the γ-coefficient, which directly depends on the divergence angle. As presented in Section 4.2, the divergence angle increases with increasing current. Due to the widening of the beam, the cosine losses increase and thus the value of the γ-coefficient decreases.

When comparing the direct and indirect measurement results, a minimally larger value for the direct measurement is again noticeable. In the nominal emitter current range (2–4 mA) of the laboratory IFM Nano Thruster version, in average a deviation of ~4.4 µN (~1.6%) can be observed for the V_{em} constant values between direct and indirect thrust. The V_{ex} constant values have in average an increased deviation of ~15.2 µN (~4.3%) in the nominal operation range. The increased deviation can be explained by increased current fluctuations that were detected during the test of the V_{ex} constant data series. For lower currents, the percentage deviation increases for both measurement series. This can again be explained with the vertical inaccuracy of the beam diagnostics system. Another explanation is the increased deviation of the integrated total beam current with lower emission current as described in Section 4.2. However, all beam diagnostics values are again within the error range of the thrust balance.

5. Conclusion

The newly developed high-precision mN-thrust balance was presented, which achieves an accuracy of less than 2 % at six different thrust magnitudes, ranging from 10 µN to 1 N. The high accuracy is archived by using voice coil actuators, which take advantage of the linear dependence of an applied current on the executed force. At the same time as the direct thrust measurements, indirect measurements were performed with our beam diagnostics system on an IFM Nano Thruster test module. By using both systems simultaneously, inaccuracies due to air cycles or system conversions could be prevented. The comparison of both systems has shown that they agree with an inaccuracy of less than 5 % for a thrust ranging from 50 to 450 µN.

The results confirm the reliability of indirect thrust measurements for FEEP thrusters. These findings will be used in our verified electrostatic beam simulation model. This enables the thrust prediction of any new FEEP thruster geometry.

Declaration of competing interest

The authors declare that they have no known competing financial interests or personal relationships that could have appeared to influence the work reported in this paper.

Acknowledgements

This document is the result of research projects funded by the European Space Agency (ESA), France under the contract 4000127152/19NL/HB and the Austrian Research Promotion Agency (FFG) under the contracts 874844 and 884120. The authors acknowledge the TU Wien Bibliothek, Austria for financial support through its Open Access Funding Program.

References

[1] L. Massotti, J.G. del Amo, P. Silvestrin, D. Krejci, A. Reissner, B. Seifert, The Next Generation Gravity Mission and the qualification of the indium-fed mN-FEEP thruster, CEAS Space J. 14 (1) (2021) 109–124, http://dx.doi.org/10.1007/s12567-021-00386-0.

[2] B. Seifert, N. Buldrini, T. Hörbe, F. Plesescu, A. Reissner, D. Krejci, P. Friedhoff, S. Lai, In-orbit demonstration of the indium-FEEP IFM nano thruster, in: 6th SPC, Seville, Spain, 2018.

[3] D. Rafalskyi, J.M. Martínez, L. Habl, E.Z. Rossi, P. Proynov, A. Boré, T. Baret, A. Poyet, T. Lafleur, S. Dudin, A. Aanesland, In-orbit demonstration of an iodine electric propulsion system, Nature 599 (7885) (2021) 411–415, http://dx.doi.org/10.1038/s41586-021-04015-y.

[4] A. Schwertheim, E.R. Azevedo, G. Liu, E.B. Borràs, L. Bianchi, A. Knoll, Interlaboratory validation of a hanging pendulum thrust balance for electric propulsion testing, Rev. Sci. Instrum. 92 (3) (2021) 034502, http://dx.doi.org/10.1063/5.0037100.

[5] A. Neumann, J. Simon, J. Schmidt, Thrust measurement and thrust balance development at DLR's electric propulsion test facility, EPJ Techn. Instrum. 8 (1) (2021) http://dx.doi.org/10.1140/epjti/s40485-021-00074-7.

[6] Z. Zhang, G. Hang, J. Qi, Z. Zhang, Z. Zhang, J. Liu, W. Yang, H. Tang, Design and fabrication of a full elastic sub-micron-Newton scale thrust measurement system for plasma micro thrusters, Plasma Sci. Technol. 23 (10) (2021) 104004, http://dx.doi.org/10.1088/2058-6272/ac1ac3.

[7] M. Kößling, M. Monette, M. Weikert, M. Tajmar, The SpaceDrive project - Thrust balance development and new measurements of the Mach-Effect and EMDrive Thrusters, Acta Astronaut. 161 (2019) 139–152, http://dx.doi.org/10.1016/j.actaastro.2019.05.020.

[8] S. Xu, Z. Zhang, Z. Zhang, W. Yang, H. Tang, W.Y.L. Ling, Time-frequency-domain method for thrust noise characteristics of electric thrusters, Acta Astronaut. 188 (2021) 308–325, http://dx.doi.org/10.1016/j.actaastro.2021.07.033.

[9] D.G. Courtney, S. Dandavino, H. Shea, Comparing direct and indirect thrust measurements from passively fed ionic electrospray thrusters, J. Propul. Power 32 (2) (2016) 392–407, http://dx.doi.org/10.2514/1.b35836.

[10] D. Krejci, F. Mier-Hicks, R. Thomas, T. Haag, P. Lozano, Emission characteristics of passively fed electrospray microthrusters with propellant reservoirs, J. Spacecr. Rockets 54 (2) (2017) 447–458, http://dx.doi.org/10.2514/1.a33531.

[11] B. Seifert, A. Reissner, N. Buldrini, F. Plesescu, Development and verification of a μn thrust balance for high voltage electric propulsion systems, in: 33rd IEPC, no. IEPC-2013-N, 2013.

[12] D. Krejci, B. Seifert, C. Scharlemann, Endurance testing of a pulsed plasma thruster for nanosatellites, Acta Astronaut. 91 (2013) 187–193, http://dx.doi.org/10.1016/j.actaastro.2013.06.012.

[13] J.E. Polk, A. Pancotti, T. Haag, S. King, M. Walker, J. Blakely, J. Ziemer, Recommended practice for thrust measurement in electric propulsion testing, J. Propul. Power 33 (3) (2017) 539–555, http://dx.doi.org/10.2514/1.b35564.

[14] N.S. Mühlich, B. Seifert, E. Ceribas, J. Gerger, F. Aumayr, High-precision digital faraday cups for FEEP thrusters, in: 72nd IAC, no. IAC-21-C4.6.13, 2021.

[15] N.S. Mühlich, B. Seifert, F. Aumayr, IFM Nano Thruster performance studied by experiments and numerical simulations, J. Phys. D: Appl. Phys. 54 (2021) 095203, http://dx.doi.org/10.1088/1361-6463/abc84c.

[16] D.M. Goebel, I. Katz, Fundamentals of Electric Propulsion: Ion and Hall Thrusters, Jet Propulsion Laboratory California Institute of Technology, 2008.

[17] M. Fehringer, F. Ruedenauer, W. Steiger, Indium liquid-metal ion sources as micronewton thrusters, AIP Conf. Proc. (1998) http://dx.doi.org/10.1063/1.57413.

[18] B. van Reijen, S. Weis, A. Lazurenko, J. Haderspeck, A. Genovese, P. Holtmann, K. Ruf, N. Püttmann, High precision thrust vector determination through full hemispherical RPA measurements assisted by angular mapping of ion energy charge state distribution, in: 33rd IEPC, 2013.

[19] N.S. Mühlich, S. Keerl, W. Engel, E. Ceribas, R.-J. Koopmans, Retarding potential analyser development for low density FEEP thruster beam diagnostics, in: 36th IEPC, no. IEPC-2019-445, 2019.

[20] F.S. Gulczinski, A.D. Gallimore, Near-field ion energy and species measurements of a 5-kW hall thruster, J. Propul. Power 17 (2) (2001) 418–427, http://dx.doi.org/10.2514/2.5758.

[21] F.G. Hey, Micro Newton Thruster Development, Springer Fachmedien Wiesbaden, 2018, http://dx.doi.org/10.1007/978-3-658-21209-4.

[22] B. Seifert, A. Reissner, N. Buldrini, T. Hörbe, F. Plesescu, A. Bulit, E. Bosch Borras, Verification of the FOTEC μn thrust balance at the esa propulsion lab, in: 34th IEPC and 30th ISTS, no. IEPC-2015-258 / ISTS-2015-b-258, 2015.

[23] V. Hugonnaud, S. Mazouffre, D. Krejci, Faraday cup sizing for electric propulsion ion beam study: Case of a field-emission-electric propulsion thruster, Rev. Sci. Instrum. 92 (8) (2021) 084502, http://dx.doi.org/10.1063/5.0060931.